Electronic Supplementary Material (ESI) for Physical Chemistry Chemical Physics.

Supporting Information on

Excited-state torsional relaxation dynamics of *meso-meso* directly linked corrole dimers: importance of liking position

Kyu Hyung Park,[†] Shota Ooi,[‡] Taeyeon Kim,[†] Takayuki Tanaka,[,‡] Atsuhiro Osuka,[*,‡] Dongho Kim,[*,†]*

[†]Spectroscopy Laboratory for Functional π - Electronic Systems and Department of Chemistry, Yonsei University, Seoul 120-749, Korea

[‡]Department of Chemistry, Graduate School of Science, Kyoto University, Sakyo-ku, Kyoto 606-8502, Japan

E-mail: dongho@yonsei.ac.kr (D. Kim); osuka@kuchem.kyoto-u.ac.jp (A. Osuka)

Table of Contents

1. Experimental details

Sample Preparation. The details in synthesis, characterization, and X-ray crystallographic analysis of **5CD** and **10CD** are described elsewhere.[1-3] The single crystals of **5CD** and **10CD** for X-ray analyses were obtained by the vapor diffusion method with $CHCl_3$/*n*-hexane and benzene/heptane, respectively.

Steady-state Measurements. Steady-state absorption spectra were measured on a UV/Vis/NIR spectrometer (Varian, Cary5000) and fluorescence spectra were measured on a fluorescence spectrophotometer (Scinco, FS-2). All spectroscopic measurements were carried out in toluene solution to ensure long term photostability of the samples.[4] HPLC-grade toluene was purchased from Sigma-Aldrich and used without further purification.

Picosecond Time-resolved Fluorescence Measurements. A time-correlated single-photon-counting (TCSPC) system was used for measurements of spontaneous fluorescence decay. As an excitation light source, we used a mode-locked Ti:sapphire laser (Spectra Physics, MaiTai BB) which provides ultrashort pulse (center wavelength of 800 nm with 80 fs at FWHM) with high repetition rate (80 MHz). This high repetition rate was reduced to 800 kHz by using homemade pulse-picker. The pulse-picked output was frequency doubled by a 1-mm-thick BBO crystal (type-I, θ = 29.2°, EKSMA). The fluorescence was collected by a microchannel plate photomultiplier (MCP-PMT, Hamamatsu, R3809U-51) with a thermoelectric cooler (Hamamatsu, C4878) connected to a TCSPC board (Becker & Hickel SPC-130). The overall instrumental response function was about 25 ps (FWHM). A vertically polarized pump pulse by a Glan-laser polarizer was irradiated to samples, and a sheet polarizer set at an angle complementary to the magic angle (54.7°), was placed in the fluorescence collection path to obtain polarization-independent fluorescence decays.

Femtosecond Transient Absorption Measurements. A femtosecond time-resolved transient absorption (TA) spectrometer used for this study consisted of a femtosecond optical parametric amplifier (Quantronix, Palitra-FS) pumped by a Ti:sapphire regenerative amplifier system (Quantronix, Integra-C) operating at 1 kHz repetition rate and an accompanying optical detection system. The

generated OPA pulses had a pulse width of ~100 fs and an average power of 1 mW in the range 580 to 690 nm, which were used as pump pulses. White light continuum (WLC) probe pulses were generated using a sapphire window (2 mm thick) by focusing of small portion of the fundamental 800 nm pulses, which were picked off by a quartz plate before entering into the OPA. The time delay between pump and probe beams was carefully controlled by making the pump beam travel along a variable optical delay (Newport, ILS250). Intensities of the spectrally dispersed WLC probe pulses were monitored by high speed spectrometer (Ultrafast Systems). To obtain the time-resolved transient absorption difference signal (ΔA) at a specific time, the pump pulses were chopped at 500 Hz and absorption spectra intensities were saved alternately with or without pump pulse. Typically, 6000 pulses were used excite samples and to obtain the TA spectra at a particular delay time. The polarization angle between pump and probe beam was set at the magic angle (54.7°) using a Glan-laser polarizer with a half-wave retarder to prevent polarization-dependent signals. The cross-correlation fwhm in the pump-probe experiments was less than 200 fs, and chirp of WLC probe pulses was measured to be 800 fs in the 450-850 nm regions. To minimize chirp, all reflection optics were used in the probe beam path, and a quartz cell of 2 mm path length was employed. After completing each set of fluorescence and TA experiments, the absorption spectra of all compounds were carefully checked to rule out the presence of artifacts or spurious signals arising from, for example, degradation or photo-oxidation of the samples in question.

2. Computational details

Quantum mechanical calculations were performed by Gaussian09 program suite.[5] Geometry optimizations were carried out by the density functional theory (DFT) method with Coulomb attenuated method Becke's three-parameter hybrid exchange functional and the Lee-Yang-Parr correlation functional (CAM-B3LYP),[6] employing a basis set containing 6-31G(d) for all atoms.[7] The X-ray crystallographic structures were used as initial geometries for geometry optimization.[2,3] To simulate the ground-state absorption spectra, we used time-dependent (TD) DFT calculations with the same functional and basis set as used in the geometry optimization.[8] Relaxed scan along inter-corrole torsional angle coordinate were carried out without pentafluorophenyl substituents to reduce the computational cost. Mulliken population analysis on corrole monomer was performed at the same level of theory with and without pentafluorophenyl groups to assure the appearance of asymmetric π-electron structure irrespective of the presence of *meso*-substituents.

3. Supporting tables and figures (Table S1–S2, Fig. S1–S7)

Table S1. Molecular Orbital Coefficients of Carbon Atoms Constituting Free-Base Corrole.

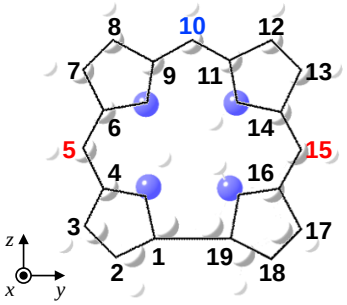

Position	Orbital type	Molecular Orbital			
		HOMO-1	**HOMO**	**LUMO**	**LUMO+1**
1	$2p_x$	-0.18764	0.13521	0.15116	-0.12946
	$3p_x$	-0.13611	0.11215	0.13424	-0.13374
2	$2p_x$	-0.15459	0.00306	0.11138	0.05334
	$3p_x$	-0.13637	0.00119	0.11896	0.06140
3	$2p_x$	0.10351	-0.11135	-0.17148	0.08201
	$3p_x$	0.09149	-0.09281	-0.18001	0.09268
4	$2p_x$	0.22822	-0.04936	-0.06005	-0.10445
	$3p_x$	0.18019	-0.04589	-0.05399	-0.12145
5	$2p_x$	0.02075	0.20715	0.24860	-0.15862
	$3p_x$	0.01589	0.18420	0.24999	-0.15459
6	$2p_x$	-0.19264	0.10876	-0.03614	0.16936
	$3p_x$	-0.15102	0.07250	-0.03881	0.16306
7	$2p_x$	-0.08073	-0.00591	-0.13119	0.15128
	$3p_x$	-0.07427	0.00250	-0.13494	0.17014
8	$2p_x$	0.09557	-0.08134	0.04683	-0.17857
	$3p_x$	0.08968	-0.06756	0.05726	-0.20008

9	$2p_x$	0.17933	-0.04102	0.16435	-0.12129
	$3p_x$	0.13161	-0.04324	0.14775	-0.11060
10	$2p_x$	0.05456	0.25160	0.08581	0.23907
	$3p_x$	0.05229	0.22354	0.09893	0.23973
11	$2p_x$	-0.14636	0.10792	-0.18805	-0.01364
	$3p_x$	-0.11582	0.07853	-0.18699	0.00456
12	$2p_x$	-0.10122	-0.09089	-0.10553	-0.19890
	$3p_x$	-0.09071	-0.07536	-0.11533	-0.22935
13	$2p_x$	0.07224	-0.09704	0.17741	0.11237
	$3p_x$	0.06562	-0.08547	0.19280	0.13116
14	$2p_x$	0.17660	0.09273	0.05657	0.18590
	$3p_x$	0.14010	0.07224	0.04613	0.18945
15	$2p_x$	-0.00191	0.23858	-0.22887	-0.12553
	$3p_x$	-0.00044	0.21188	-0.23036	-0.12957
16	$2p_x$	-0.20401	-0.05300	0.05589	-0.12417
	$3p_x$	-0.16740	-0.04754	0.04390	-0.14657
17	$2p_x$	-0.09390	-0.12679	0.14451	0.07592
	$3p_x$	-0.08324	-0.11516	0.15604	0.08839
18	$2p_x$	0.14114	0.00517	-0.10349	0.07045
	$3p_x$	0.12599	0.01203	-0.11420	0.08131
19	$2p_x$	0.16928	0.14860	-0.12237	-0.13140
	$3p_x$	0.12192	0.12816	-0.10380	-0.14369

Table S2. Molecular Orbital Coefficients of Carbon Atoms Constituting Free-Base Corrole Tautomer.

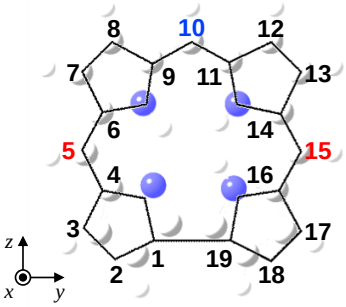

Position	Orbital type	Molecular Orbital			
		HOMO-1	**HOMO**	**LUMO**	**LUMO+1**
1	$2p_x$	0.13625	0.15906	0.18211	-0.11650
	$3p_x$	0.10029	0.12026	0.15418	-0.10543
2	$2p_x$	0.09879	0.07223	0.14074	-0.00411
	$3p_x$	0.08737	0.06603	0.15373	-0.00953
3	$2p_x$	-0.05658	-0.08458	-0.17055	0.08930
	$3p_x$	-0.05536	-0.07390	-0.18017	0.09561
4	$2p_x$	-0.17016	-0.15187	-0.13640	-0.02770
	$3p_x$	-0.12189	-0.12740	-0.13051	-0.03047
5	$2p_x$	-0.16163	0.11135	0.23611	-0.19645
	$3p_x$	-0.14269	0.09737	0.23266	-0.20074
6	$2p_x$	0.11986	0.20080	0.05291	0.12926
	$3p_x$	0.10011	0.15804	0.05964	0.12524
7	$2p_x$	0.12718	0.03135	-0.13295	0.16032
	$3p_x$	0.10794	0.03293	-0.13981	0.17562
8	$2p_x$	-0.04763	-0.15355	-0.00367	-0.17907
	$3p_x$	-0.04429	-0.13663	-0.00306	-0.19986
9	$2p_x$	-0.18125	-0.09987	0.16154	-0.09543

	$3p_x$	-0.13996	-0.08041	0.16185	-0.08195
	$2p_x$	-0.08989	0.22367	0.07460	0.24227
10					
	$3p_x$	-0.08043	0.19577	0.08012	0.24434
	$2p_x$	0.13909	0.13202	-0.18177	-0.04989
11					
	$3p_x$	0.11253	0.10513	-0.18236	-0.03095
	$2p_x$	0.11727	-0.08546	-0.07500	-0.21020
12					
	$3p_x$	0.10437	-0.07260	-0.08368	-0.24175
	$2p_x$	-0.06538	-0.11396	0.16667	0.14135
13					
	$3p_x$	-0.05951	-0.10072	0.18310	0.16231
	$2p_x$	-0.19086	0.08040	0.01432	0.18220
14					
	$3p_x$	-0.15310	0.06334	0.00282	0.18240
	$2p_x$	-0.01167	0.23030	-0.20511	-0.16997
15					
	$3p_x$	-0.01011	0.20470	-0.20494	-0.17719
	$2p_x$	0.21586	-0.04102	0.09221	-0.09505
16					
	$3p_x$	0.17505	-0.03831	0.08155	-0.11234
	$2p_x$	0.11405	-0.10606	0.13626	0.08917
17					
	$3p_x$	0.10308	-0.09736	0.14633	0.10249
	$2p_x$	-0.13731	0.00001	-0.12920	0.04035
18					
	$3p_x$	-0.12353	0.00633	-0.14146	0.04417
	$2p_x$	-0.19789	0.12525	-0.11057	-0.12485
19					
	$3p_x$	-0.14918	0.11358	-0.08257	-0.13978

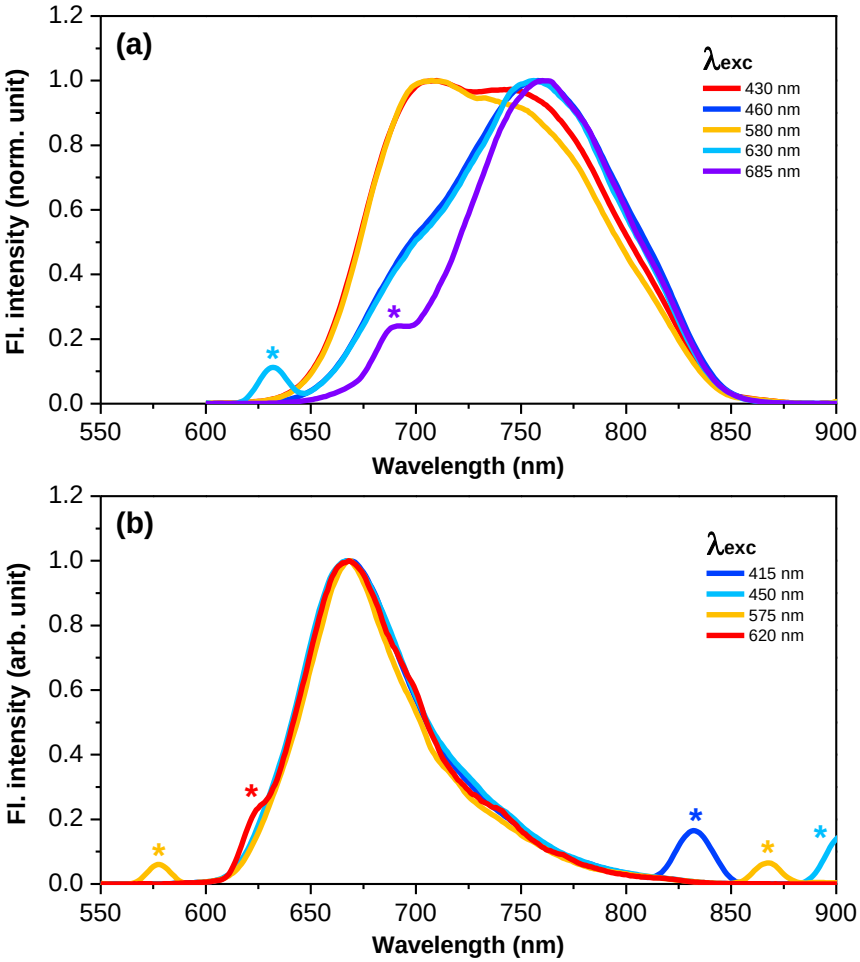

Fig. S1 Steady-state fluorescence spectra of (a) **5CD** and (b) **10CD** in toluene obtained at various excitation wavelengths. All spectra are normalized to help comparing the spectral shapes and positions.

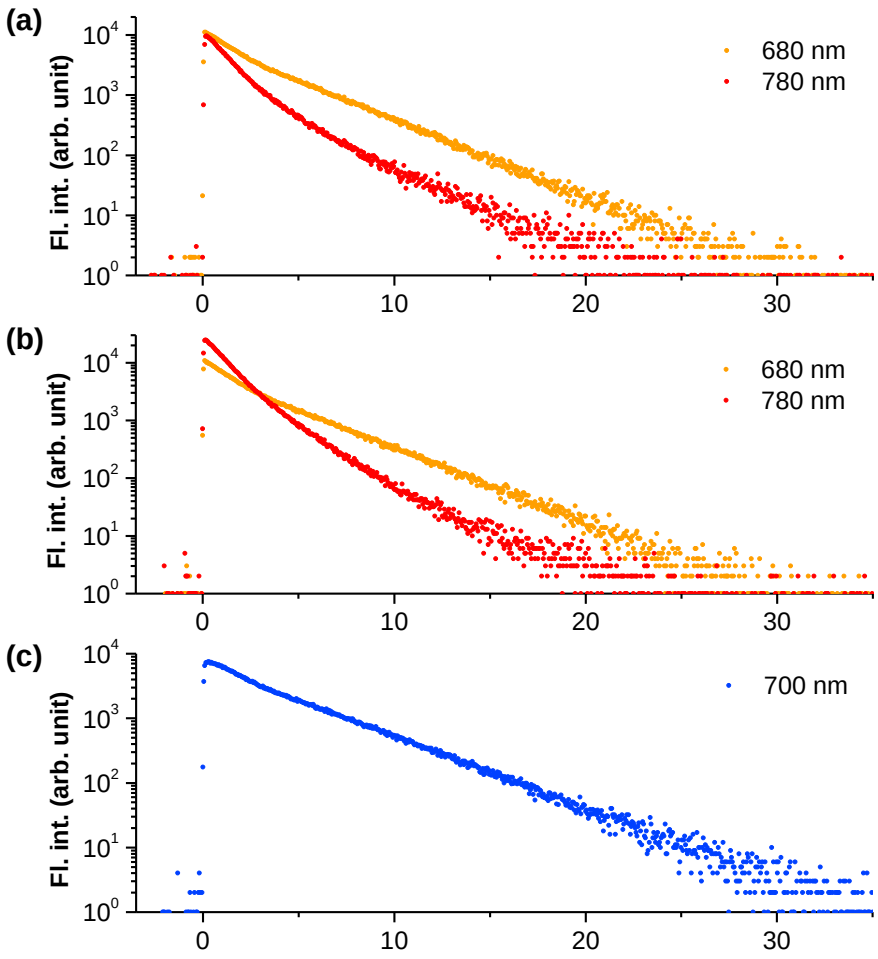

Fig. S2 Nanosecond fluorescence decay profiles of (a) **5CD** upon photoexcitation at 430 nm, (b) **5CD** upon photoexcitation at 460 nm, and (c) **10CD** upon photoexcitation at 415 nm. Probe wavelengths are indicated.

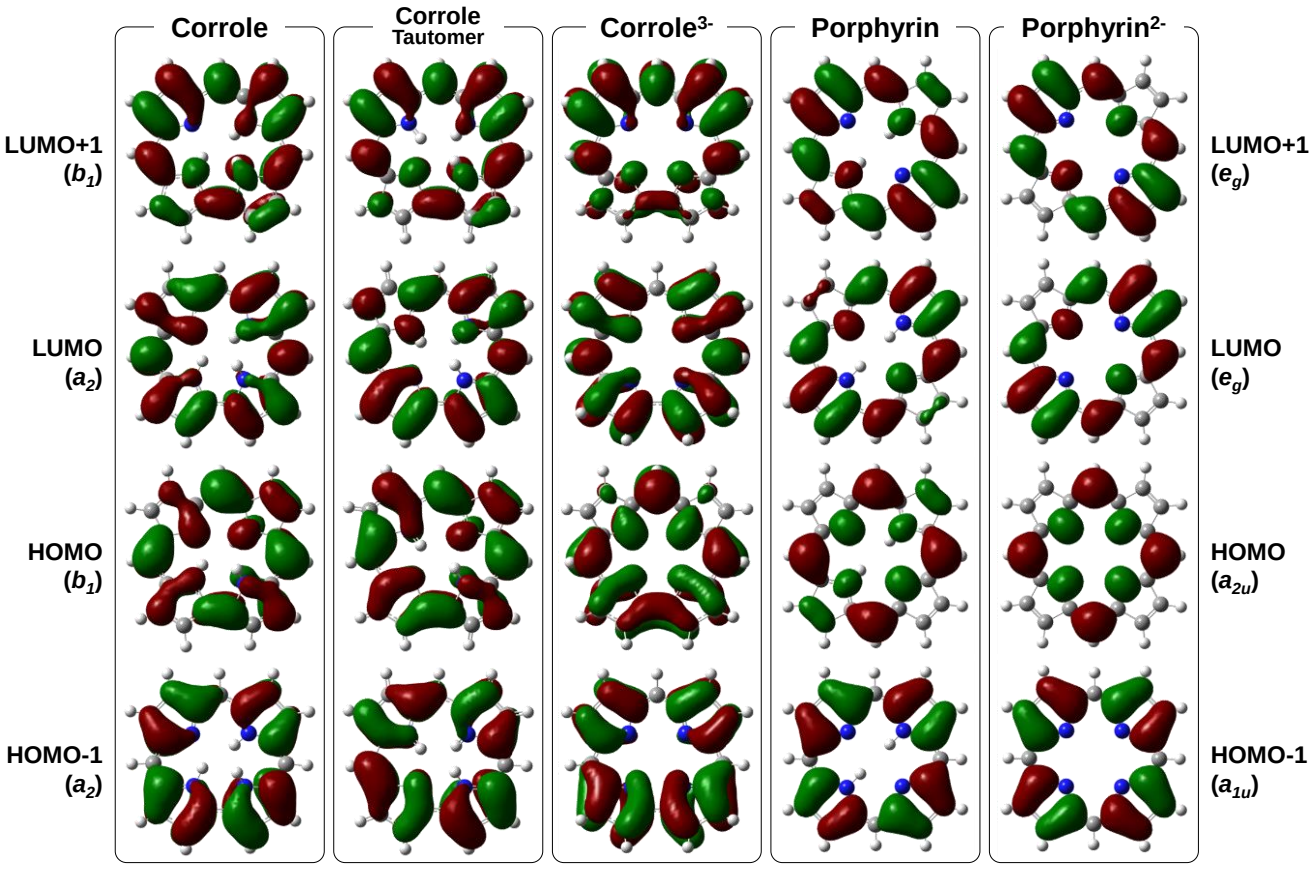

Fig. S3 Four frontier orbitals of corrole, corrole tautomer, corrole trianion, porphyrin, and porphyrin dianion calculated at CAM-B3LYP/6-31G(d) level.

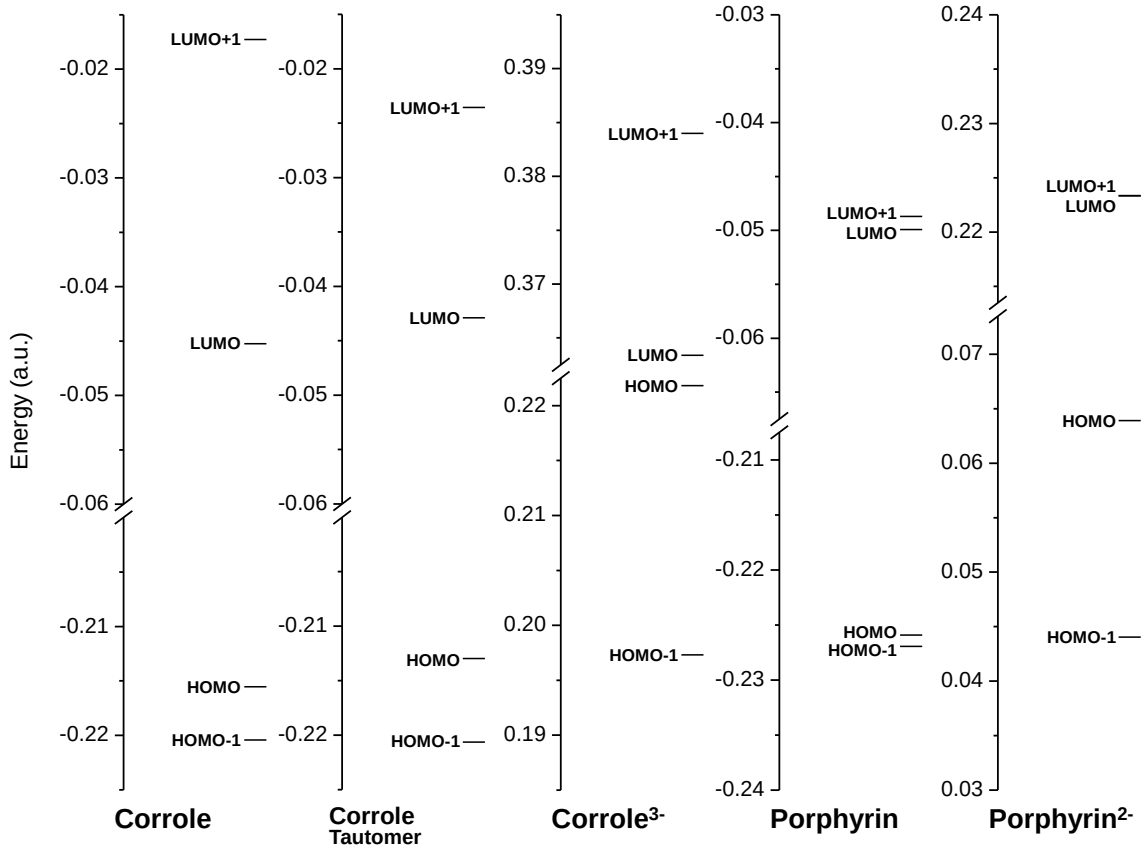

Fig. S4 Energy level diagrams of corrole, corrole tautomer, corrole trianion, porphyrin, and porphyrin dianion calculated at CAM-B3LYP/6-31G(d) level.

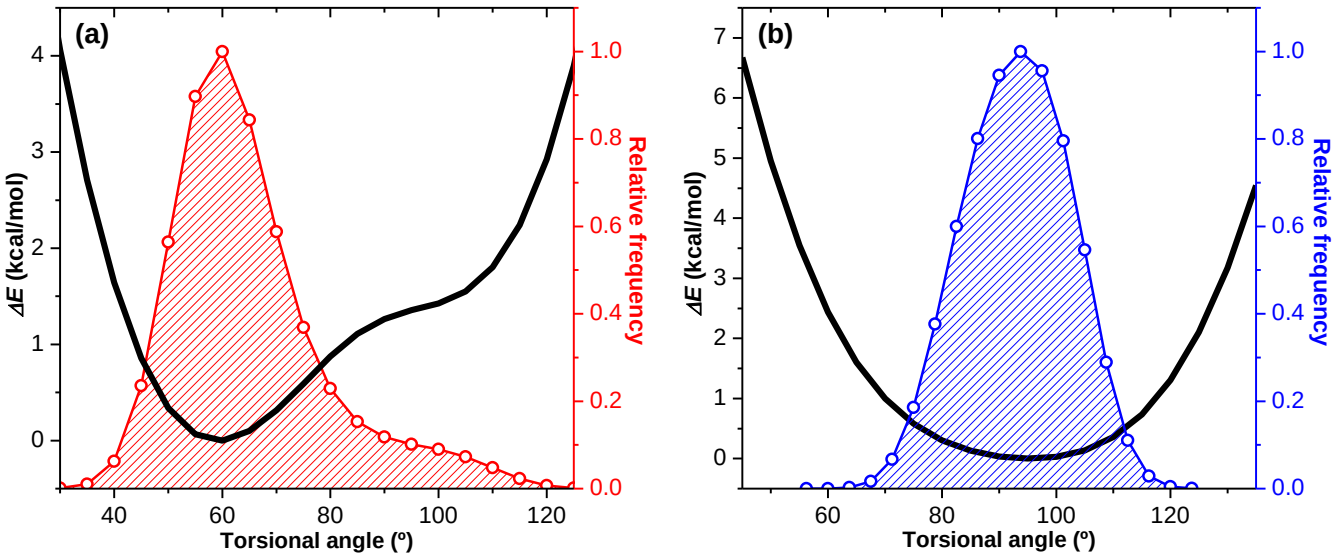

Fig. S5 Ground state potential curves along inter-corrole torsional angle coordinate and corresponding Boltzmann distributions of (a) **5CD** and (b) **10CD** calculated at CAM-B3LYP/6-31G(d) level.

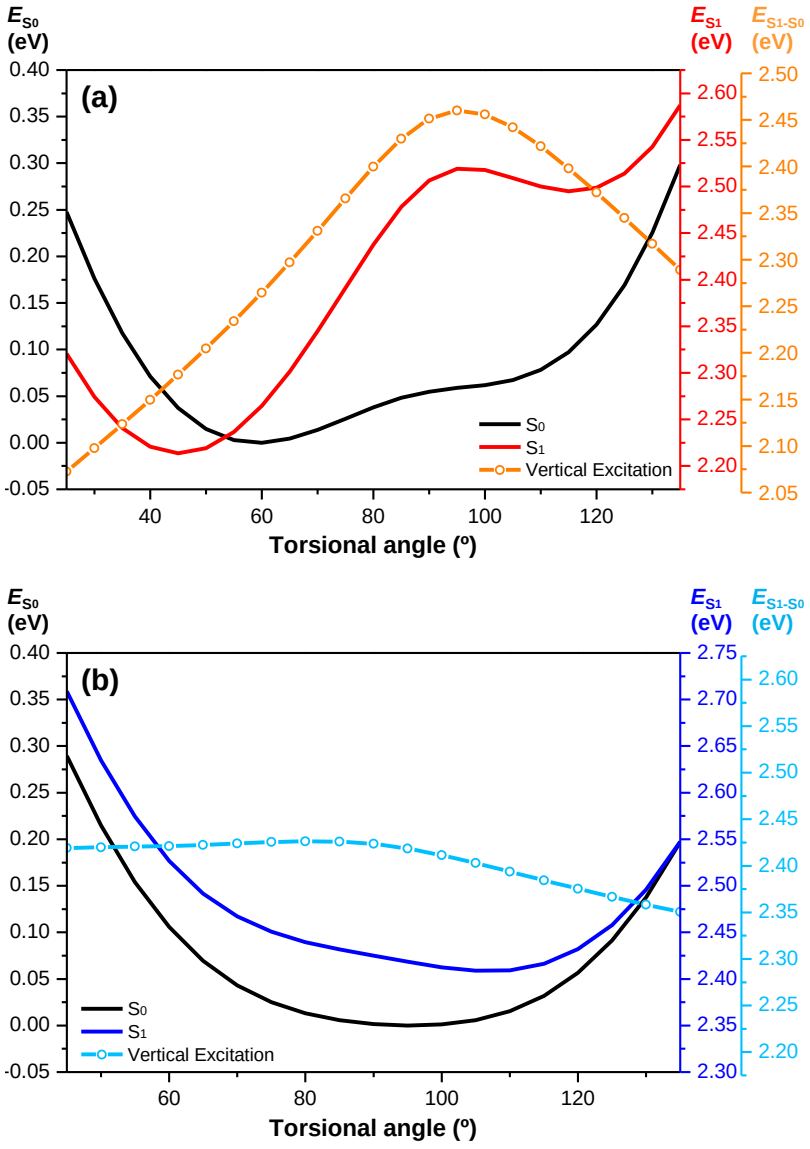

Fig. S6 Ground and the first excited-state potential curves plotted with the vertical excitation energies of (a) **5CD** and (b) **10CD** along inter-corrole torsional angle coordinate. All energies were calculated at CAM-B3LYP/6-31G(d) level.

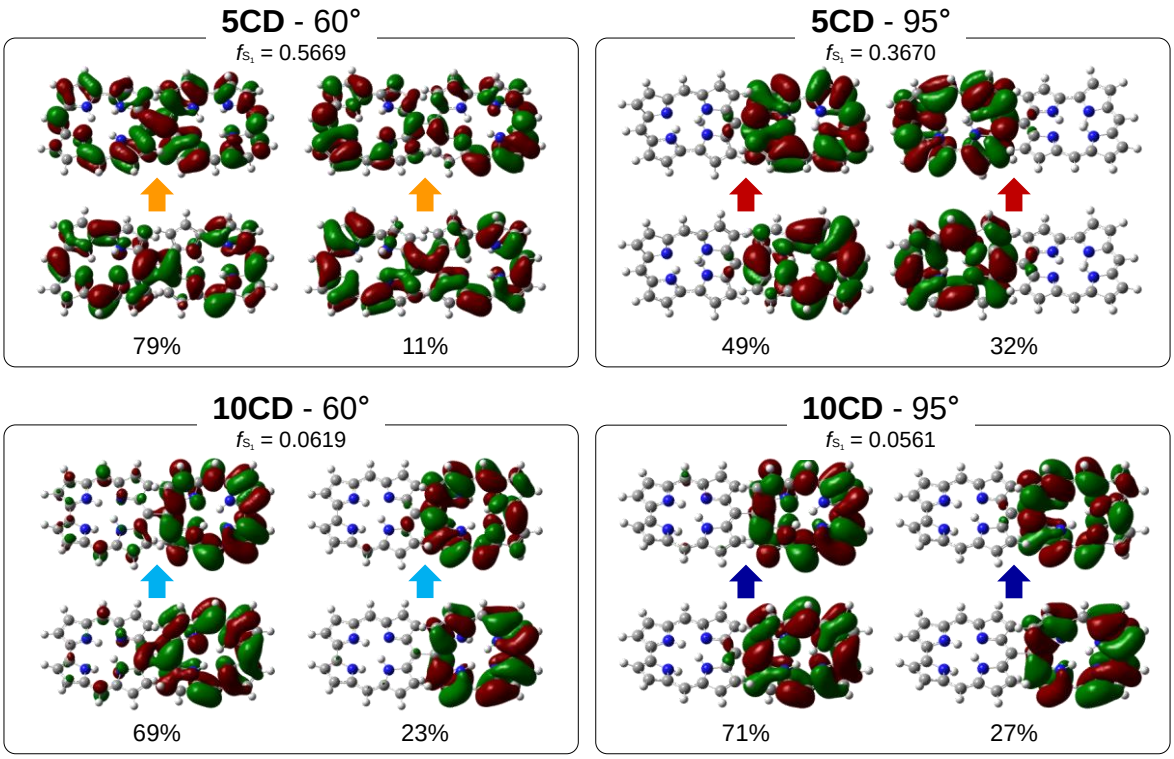

Fig. S7 Dominant natural transition orbitals (NTOs) of **5CD** (top row) and **10CD** (bottom row) with inter-corrole torsional angle of 60° (left column) and 95° (right column). Contribution of each set of transition to total transition is indicated in percentage.

4. References

(1) S. Ooi, T. Yoneda, T. Tanaka and A. Osuka, *Chem. Eur. J.*, 2015, **21**, 7772.

(2) S. Ooi, T. Tanaka, K. H. Park, D. Kim and A. Osuka, *Angew. Chem. Int. Ed.*, 2016, **55**, DOI: 10.1002/anie.201601864

(3) S. Ooi, T. Tanaka, K. H. Park, S. Lee, D. Kim and A. Osuka, *Angew. Chem. Int. Ed.*, 2015, **54**, 3107.

(4) B. Ventura, A. D. Esposti, B. Koszarna, D. T. Gryko and L. Flamigni, *New J. Chem.*, 2005, **29**, 1559.

(5) M. J. Frisch, G. W. Trucks, H. B. Schlegel, G. E. Scuseria, M. A. Robb, J. R. Cheeseman, G. Scalmani, V. Barone, B. Mennucci, G. A. Petersson, H. Nakatsuji, M. Li, X. Caricato, H. P. Hratchian, A. F. Izmaylov, J. Bloino, G. Zheng, J. L. Sonnenberg, M. Hada, M. Ehara, K. Toyota, R. Fukuda, J. Hasegawa, M. Ishida, T. Nakajima, Y. Honda, O. Kitao, H. Nakai, T. Vreven, J. A. Montgomery, J. E. Peralta, F. Ogliaro, M. Bearpark, J. J. Heyd, E. Brothers, K. N. Kudin, V. N. Staroverov, R. Kobayashi, J. Normand, K. Raghavachari, A. Rendell, J. C. Burant, S. S. Iyengar, J. Tomasi, M. Cossi, N. Rega, J. M. Millam, M. Klene, J. E. Knox, J. B. Cross, V. Bakken, C. Adamo, J. Jaramillo, R. Gomperts, R. E. Stratmann, O. Yazyev, A. J. Austin, R. Cammi, C. Pomelli, J. W. Ochterski, R. L. Martin, K. Morokuma, V. G. Zakrzewski, G. A. Voth, P. Salvador, J. J. Dannenberg, S. Dapprich, A. D. Daniels, Ö. Farkas, J. B. Foresman, J. V. Ortiz, J. Cioslowski and D. J. Fox, Gaussian 09, revision A.1; Gaussian Inc.; Wallingford CT, 2009 2 BrukerAXS. (2007-2013) APEX2 (Ver. 2013.2-0), SADABS (2012-1), and SAINT+ (Ver. 8.30C) Software Reference Manuals. Bruker-AXS, Madison, Wisconsin, USA.

(6) T. Yanai, D. P. Tew, N. C. Handy, *Chem. Phys. Lett.*, 2004, **393**, 51.

(7) R. Ditchfield, W. J. Hehre, J. A. Pople, *J. Chem. Phys.*, 1971, **54**, 724.

(8) R. Bauernschmitt, R. Ahlrichs, *Chem. Phys. Lett.*, 1996, **256**, 454.